Journal of the European Ceramic Society 21 (2001) 2453–2461

www.elsevier.com/locate/jeurceramsoc

Refinement of the real structures of 2:1 and 3:2 mullite

S. Freimann*, S. Rahman

Institut für Mineralogie, Universität Hannover, Welfengarten 1, 30167 Hannover, Germany

Abstract

In a previous investigation (Rahman, S. H., Strothenk, S., Paulmann, C. and Feustel, U., Interpretation of mullite real structure via inter-vacancy correlation vectors. *J. Eur. Ceram. Soc.*, 1996, **16**, 177–186) we showed that the real structure of 2:1 mullite can be explained with intervacancy correlation vectors and a 3D ordering scheme for the oxygen vacancies was derived. This ordering scheme is now refined by varying the frequencies of the most important 3D vectors in videographic 3D simulations, which are tested through comparison between their Fourier transforms with the experimental diffraction patterns for the planes h0l, 0kl, hk1/2, hk1/3, hk1/4 and hk1/6. The best agreement with the experimental patterns of 2:1 mullite was reached by a 3D simulation that can be described by the following sequence of the most frequent correlation vectors *lmn* ($l=a/2$, $m=b/2$, $n=c$): ⟨310⟩, ⟨111⟩, ⟨022⟩, ⟨201⟩, ⟨330⟩, ⟨401⟩, ⟨131⟩, ⟨130⟩, ⟨042⟩, ⟨113⟩, ⟨060⟩. The experimental single crystal diffraction patterns of 3:2 and 2:1 mullite generally show similar diffuse scattering phenomena, though the diffuse components of 3:2 mullite are slightly broadened and have weaker relative intensities. Employing videographic 3D simulations it was confirmed that the real structure of 3:2 mullite can be characterized via the same correlation vectors, but with different sequence and frequencies: ⟨022⟩, ⟨201⟩, ⟨111⟩, ⟨310⟩, ⟨130⟩, ⟨131⟩, ⟨223⟩, ⟨330⟩, ⟨222⟩, ⟨240⟩, ⟨113⟩. With the aid of the above-mentioned frequencies of correlation vectors the real structures of 2:1 and 3:2 mullite can be completely described and all the complicated diffuse scattering phenomena can be explained. Furthermore the dependence on direction of several physical properties e.g. thermal heat expansion can be interpreted by means of the vacancy distribution in the real structure.

Keywords: Diffuse scattering; Mullite; Real structure

1. Introduction

The alumosilicate mullite $Al_2[Al_{2+2x}Si_{2-2x}]O_{10-x}$ exhibits complicated diffuse scattering in nearly all reciprocal planes due to ordering processes of the oxygen vacancies and atomic shifts near the vacancy positions (Fig. 1). Because the real structure influences many physical properties and hence the knowledge of the real structure could explain e.g. the dependence on direction of several physical properties (thermal heat expansion), many investigations about the real structure of mullite were performed.

In the past, many authors[2–4] assumed an incommensurate modulation of the 2:1 mullite structure with a doubling of the *c*-lattice constant and an incommensurate period along the *a*-axis, interpreting diffuse maxima in the h0l plane (Fig. 4) as satellite reflections, which can only exist in a state of maximal ordering. However, the diffraction pattern of the 0kl plane[1] (Fig. 4) exhibits diffuse maxima at the approximate positions 0, $2k\pm2/3$, $1\pm1/5$, which does not agree with a doubling of the *c*-lattice constant. Furthermore there exist many other diffuse figures, for example cross-shaped streaks in the 0kl plane and many complicated diffuse scattering phenomena (diffuse maxima, diffuse circles and diffuse streaks) in reciprocal planes perpendicular to c^* of 2:1 mullite (Fig. 5). Since there is more diffuse scattering in reciprocal space with considerable intensities and no sharp satellite reflections it can be concluded, that the diffuse scattering in mullite is caused by short-range ordering of the oxygen vacancies coupled with atomic displacements.

An approach to describe the real structure of mullite with intervacancy correlation vectors was made 1991 by Rahman.[5] Using the videographic method, a computer-aided procedure to simulate and reconstruct the real structure in the case of disorder phenomena, 2D simulations were performed for the ab-plane preferring the intervacancy vectors ⟨310⟩ and ⟨130⟩. These videographic simulations showed in their Fourier transforms the diffuse circles of the hk1/3 and hk1/4 plane. In a recent investigation[1,6] we confirmed, that the ordering scheme of the oxygen vacancies can be described via intervacancy correlation vectors (short-range order). By

* Corresponding author.
E-mail address: s.freimann@mineralogie.uni-hannover.de (S. Freimann).

0955-2219/01/$ - see front matter
PII: S0955-2219(01)00385-5

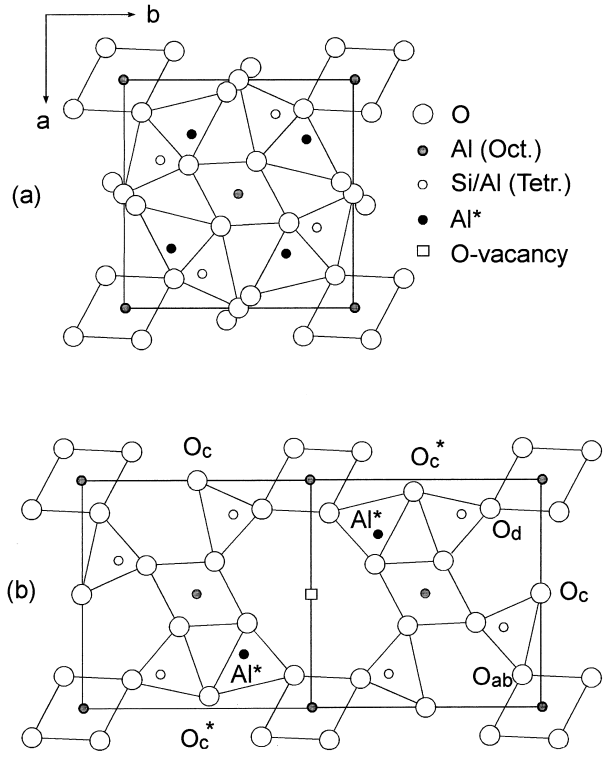

Fig. 1. Structure of mullite: (a) average structure[13]; (b) atomic displacements around an oxygen vacancy.

2D videographic simulations for the 3 main planes the frequencies of 2D correlation vectors were determined. Comparing these 2D vectors the most important 3D vectors were derived and tested with 3D videographic simulations. The 3D videographic simulations showed correct Fourier transforms for the planes h0l, 0kl and hk1/2, therefore it could be assumed that the derived ordering scheme was generally right. However, since the calculated diffraction patterns for the planes hk1/3, hk1/4 and hk1/6 differed slightly from the experimental patterns, there still remained some uncertainties about the exact frequencies of the preferred correlation vectors.

Butler and Welberry[7] calculated SRO parameters of mullite from the intensities of the diffuse scattering. The diffuse scattering was measured in the area hkl with $h,k < 4.5$ and $0.5 < l < 1.0$ and it was analyzed using least-squares techniques by deriving an equation for the diffuse scattering that only involves the local order of the oxygen vacancies. The calculated diffraction pattern of a Monte Carlo simulation, in which 12 interaction energies were adjusted to fit 12 of the 18 presented SRO parameters, are similar to the experimental pattern but still show some differences. The other SRO parameters in the simulation field were not checked, neither the Fourier transforms for the h0l and 0kl plane were given. In a following investigation using the same method Welberry and Butler[8] added two further SRO parameters to the 18, however, simulations were not performed.

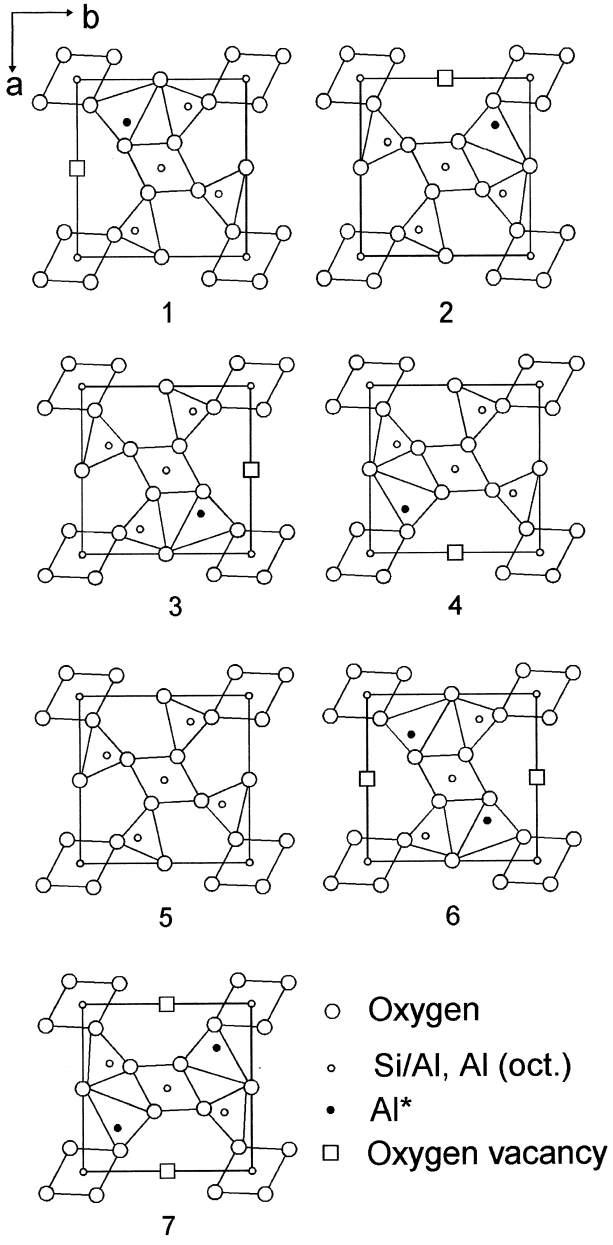

Fig. 2. Seven structure variants of mullite (neglecting the O_c* position).

The aim of the present study is to give a complete description of the real structure, that can explain all diffuse scattering phenomena in mullite. For 2:1 mullite our previous results had to be refined, in order to obtain a simulation with a good agreement in all calculated diffraction patterns. In a second step the real structure of 3:2 mullite was also refined. For both examinations the videographic method[9,10] was used, which will be briefly outlined in the following.

2. The videographic method

The videographic method is a simulation and reconstruction procedure based on a statistical mathematical

approach and computer graphics to aid the interpretation of X-ray-, electron- or neutron-diffraction from a disordered crystal. The real structure is represented as a computer graphic with different atoms replaced by picture elements (Pixel) of different grey levels according to their scattering power. The videographic method consists of two parts, the videographic simulation and the videographic reconstruction. In the present investigation only the videographic simulation procedure was used.

For the videographic simulation of a real structure first structure variants φ_j are derived from the average structure $\langle\varphi\rangle$,

$$\langle\varphi(x, y, z)\rangle = \frac{1}{N}\sum_{j=1}^{n}\varphi_j(x, y, z)\cdot N_j, \quad (1)$$

with N = total number of unit cells
N_j = number of the structure variants j.

These structure variants are distributed using combination probabilities—for the direct combination along a, b or c- and influence factors for any correlation vectors,

$$S(L, M, N) = \sum_{l}^{L}\sum_{m}^{M}\sum_{n}^{N}\varphi_{lmn}(J_{lmn}), \quad (2)$$

with $\varphi_{lmn}(J_{lmn})$ = structure variant of type J at an lmn position
J_{lmn} = random variable for an lmn position
l, m, n = integers.

The generated simulation field $S(L,M,N)$ can be displayed as videographic image by replacing every structure variant by a videographic Pixel pattern. Then the Fourier transformation of the real structure image is calculated and displayed. The simulations are tested by the agreement of their Fourier transforms with the experimental diffraction patterns. The input parameters are systematically varied until a best fit between simulation and experiment is reached. In a further step the simulation field is analyzed to obtain the frequencies of correlation vectors lmn ($l = a/2$, $m = b/2$, $n = c$).

The structure variants are derived from the average structure considering crystal chemical rules as bond lengths, atomic distances and number of coordination. The mullite structure consists of chains of edge-sharing AlO_6 octahedra along [001] which are cross-linked by (Si, Al) tetrahedral double chains. Oxygen vacancies occur on the O_c positions at the edges of the unit cell (Fig. 1). The occupation of the tetrahedral Si/Al and Al* sites depends on the position of oxygen atoms or vacancies. If the O_c site is occupied, the two adjacent Si/Al sites are occupied too. However, next to a vacancy the adjacent Al* sites are occupied instead of the Si/Al sites, and the coordinating oxygen atoms shift from the O_c to the O_c* position. Fig. 2 shows 7 structure variants for mullite which differ in the position of oxygen vacancies. The variants 1–4 have one vacancy on one edge of the unit cell, in variant 5 all O_c positions are occupied and variants 6 and 7 have two vacancies on opposite edges. There are no structure variants with two vacancies building the correlation vector ⟨110⟩, because an Al or Si atom would only be 3-fold coordinated. In these 7 variants the O_c* positions are neglected, considering the O_c* positions 34 structure variants are resulting.[1] Since the occupation of the O_c* site is coupled with the occurence of vacancies, it is possible to generate a simulation field with the 7 structure variants and subsequent convert the 7 into the 34 different variants. In this way the Fourier transforms of the videographic simulations are calculated for the correct representation of the structure.

Whereas for the calculation of the Fourier transforms for the h0l and 0kl plane of a 3D simulation the simulation field is projected along the a- or b-axis, respectively, the Fourier transforms for the planes hk1/2, hk1/3, hk1/4 and hk1/6 are determined by converting the whole simulation field into a "floating point" atomic file. This file contains the x, y, z parameters and the temperature factors. Every structure variant in the field is assigned to the corresponding atomic parameter file. The positions of the atoms contained in the atomic files of the variants are converted according to the position of the variant in the simulation field into atomic positions relating to the supercell (simulation field). For this atomic file of the supercell the structure factors F_{hkl} can be calculated for every reciprocal plane conventionally.

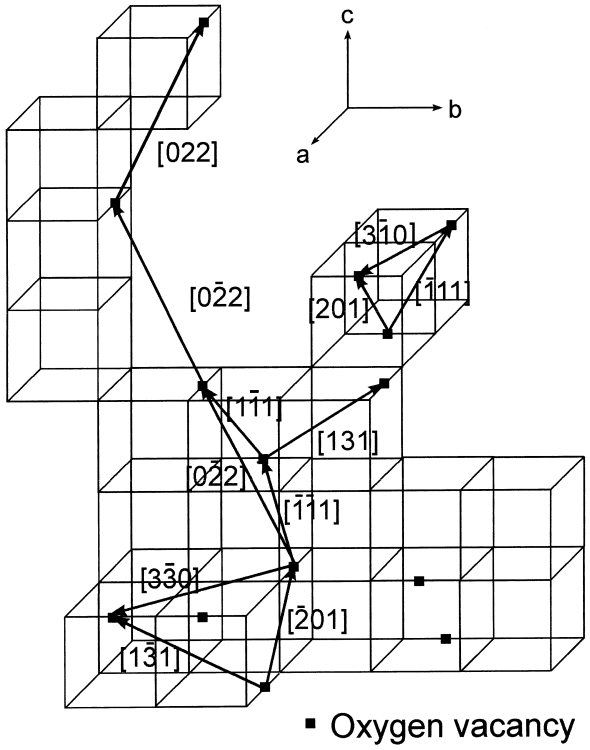

Fig. 3. 3D ordering scheme of the oxygen vacancies.

3. Refinement of the real structure of 2:1 mullite

Starting point of the refinement was the 3D ordering scheme determined earlier[1,6] This ordering scheme (Fig. 3) contains the most important 3D vectors: In the ab-plane ⟨310⟩, ⟨330⟩ and ⟨130⟩, between two neighbouring layers ⟨111⟩, ⟨201⟩ and ⟨131⟩ and between two layers in the distance of 2c the vector ⟨022⟩. It can be noticed, that combinations of the presented 3D vectors give preferred correlation vectors, too. For example the combination of the vectors [−11] and [310] results in the vector [201], the combination of [−201] and [3−30] gives [1−31] and from the combination of two different ⟨111⟩ vectors the vector ⟨022⟩ can result.

The ordering scheme was tested with the aid of videographic 3D simulations, in which the above-mentioned vectors were favoured. The first simulations showed correct Fourier transforms for the planes h0l, 0kl and hk1/2, however, in particular the calculated hk1/4 plane did not agree well with the experimental pattern. Because of the good agreement of the Fourier transforms for h0l, 0kl and hk1/2 it could be assumed, that the ordering scheme is right, but the exact frequencies of correlation vectors were probably not correct in these simulations. For this reason the frequencies of the most frequent vectors were systematically varied in the following simulations in order to refine the real structure model. Finally one 3D simulation prooved to be right, because its Fourier transforms for all reciprocal planes showed good agreement to the experimental patterns (Figs. 4 and 5).

In Fig. 4 X-ray precession patterns of the h0l and 0kl plane of 2:1 mullite (top) are presented together with the calculated diffraction patterns from the 3D simulation (bottom). In both the X-ray precession pattern and the Fourier transform of the h0l plane there are the rounded streaks with the maximum intensities at the approximate positions 1.3 a^* and 0.5 c^*. In the calculated 0kl plane the cross-shaped streaks and the diffuse maxima agree

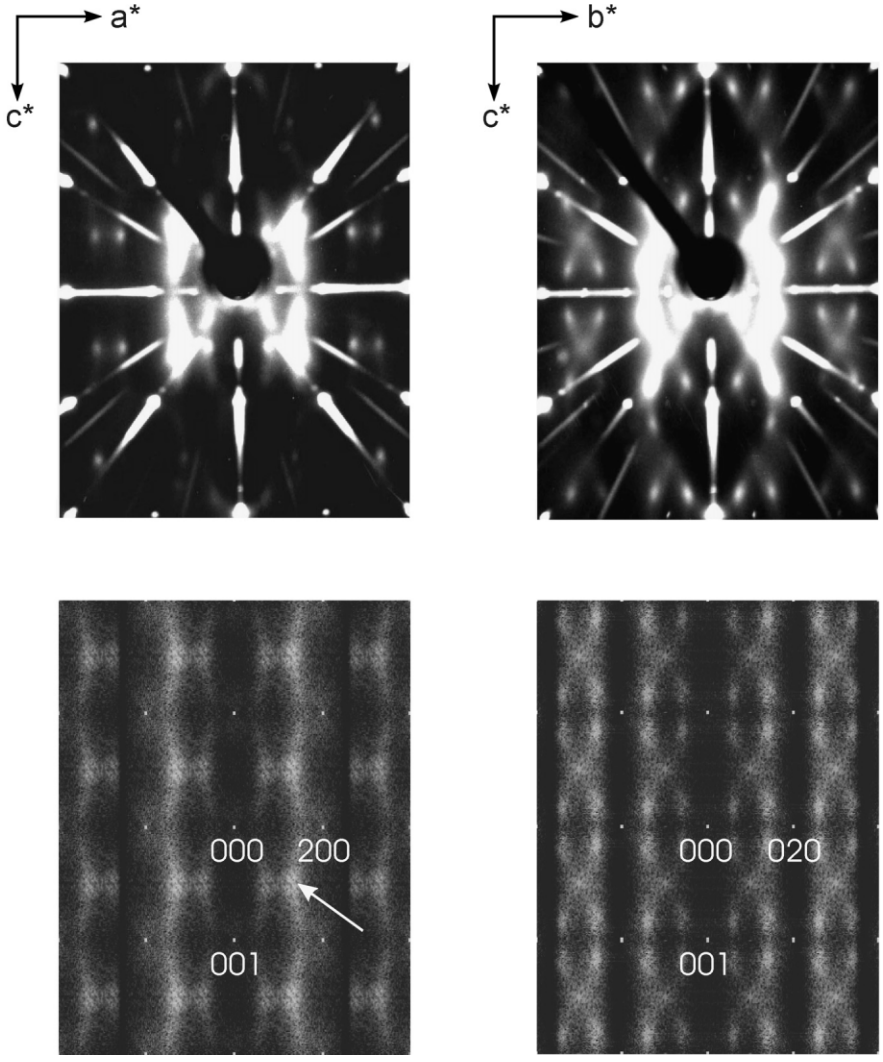

Fig. 4. (Top) X-ray diffraction patterns h0l and 0kl of 2:1 mullite (precession photograph, MoK_α); (bottom) Fourier transforms h0l and 0kl of the 3D simulation of 2:1 mullite. (The arrow indicates the maximum intensity at the position 1.3a^* and 0.5c^*.)

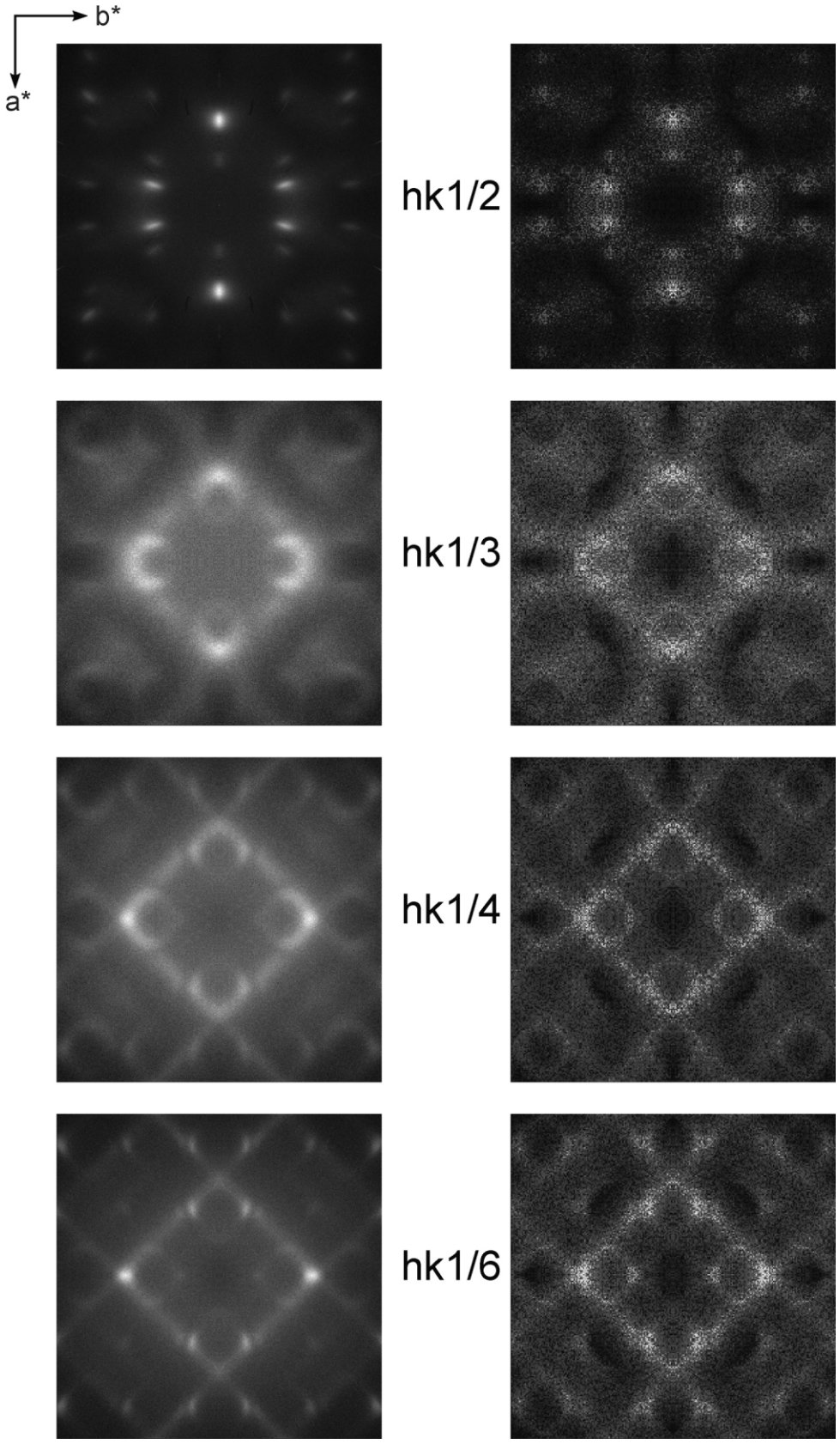

Fig. 5. (Left) X-ray diffraction patterns of 2:1 mullite; (right) Fourier transforms of the 3D simulation of 2:1 mullite.

in position and relative intensity distribution with the precession pattern. The differences at greater scattering angles may result from the fact, that the calculated Fourier transform do not include the dependence of intensity on the scattering angle.

In order to compare the agreement in the reciprocal planes perpendicular to c^*, on the left of Fig. 5 the experimental diffraction patterns of 2:1 mullite are presented and on the right the Fourier transforms for the 3D simulation are shown. In all these planes a very good agreement is observed. The calculated hk1/2 plane shows the diffuse maxima at the correct position on the a-axis at $1.3a^*$, corresponding to the diffuse maxima in the h0l plane. In the hk1/3 plane the maximum intensities are at the same position but additionally diffuse circles around the reciprocal coordinates 101/3 and 011/3 appear. In the hk1/4 plane the diffuse circles change into angular shapes and there are streaks parallel to the direction ⟨110⟩*, which are present in the hk1/6 plane, too. In both the hk1/4 and hk1/6 planes the maxima of intensity are on the b^*-axis at approximately $1.4b^*$.

Because of the good agreement between the Fourier transforms and the experimental patterns this 3D simulation gives a good representation of the vacancy distribution in 2:1 mullite. The simulation field was analyzed for all correlation vectors l, m, $n \leqslant 6$. Hence the simulation and the real structure can be completely described. The most frequent correlation vectors of the final 3D simulation are listed in Table 1 on the left. It is worth noting that the preferred vectors, contained in the 3D ordering scheme, indeed have the highest frequencies (⟨310⟩, ⟨111⟩, ⟨022⟩, ⟨201⟩, ⟨330⟩).

For some of the vectors it was possible to describe their importance for specific details of the diffuse scattering: For example the diffuse maxima in the h0l and hk1/2 plane can be explained with the vectors ⟨310⟩ and ⟨022⟩, in which ⟨310⟩ is responsible for the location along the a^*-axis at $1.3a^*$ and ⟨022⟩ for the location along the c^*-axis at $1/2c^*$.

Table 1
The most frequent correlation vectors lmn in the 3D-simulations for 2:1- and 3:2-mullite (P = probability to find at the end of a lmn correlation vector also an oxygen vacancy)

2:1- *lmn*	Mullite *p* in%	3:2- *lmn*	Mullite *p* in%
⟨310⟩	30,30	⟨022⟩	24,95
⟨111⟩	28,49	⟨201⟩	21,26
⟨022⟩	28,36	⟨111⟩	20,48
⟨201⟩	28,33	⟨310⟩	19,16
⟨330⟩	28,23	⟨130⟩	17,40
⟨401⟩	26,15	⟨131⟩	16,10
⟨131⟩	25,53	⟨223⟩	15,55
⟨130⟩	25,21	⟨330⟩	15,17
⟨042⟩	23,33	⟨222⟩	14,93
⟨113⟩	23,28	⟨240⟩	14,76
⟨060⟩	23,22	⟨113⟩	14,44
⟨600⟩	23,17	⟨312⟩	14,36
⟨312⟩	22,74	⟨401⟩	14,07
⟨222⟩	22,68	⟨153⟩	13,96
⟨040⟩	22,48	⟨004⟩	13,77

4. Refinement of the real structure of 3:2 mullite

Because of the lack of 3:2 mullite single crystals for X-ray investigations it was not possible to obtain diffraction patterns (four-circle diffractometer) for all reciprocal planes as in the case of 2:1 mullite. In order to overcome these difficulties Brunauer et al.[11] prepared a 3:2 mullite single crystal from a sillimanite single crystal by slowly thermal heating and annealing at 1600 °C for 24 h. The single crystal diffraction patterns for the planes hk1/2, hk1/3, hk1/4 and hk1/6 of this 3:2 mullite are shown on the left in Fig. 6. In comparison with the diffraction pattern of 2:1 mullite (Fig. 5) it can be noticed that both compositions (2:1 and 3:2 mullite) in principle show the same scattering phenomena, however, the diffuse figures of 3:2 mullite are broadened and have weaker relative intensities. Furthermore the exact positions of the maxima of intensity are slightly different in 2:1 and 3:2 mullite.

Because of the similar diffraction patterns of 3:2 mullite we supposed the results for 2:1 mullite to be also valid for 3:2 mullite. Thus 3D simulations for 3:2 mullite were performed preferring the same correlation vectors but with reduced frequencies because of the lower concentration of vacancies. Again the simulation was refined by varying the frequencies of the preferred vectors until the Fourier transforms of the simulation showed best agreement with the experimental diffraction patterns. In Fig. 6 on the left the experimental diffraction patterns of 3:2 mullite are presented and on the right the calculated patterns from the 3D simulation are shown. The shapes and the maximum intensities of the diffuse scattering are very similar in the experiment and the simulation.

The simulation field was analyzed and the most frequent vectors are presented in Table 1. Comparing the most frequent correlation vectors in this simulation with those for 2:1 mullite, the same correlation vectors are found for both compositions. There are only small differences in the sequence of correlation vectors (the sequence of 2:1 mullite: ⟨310⟩, ⟨111⟩, ⟨022⟩, ⟨201⟩, ⟨330⟩; the sequence of 3:2 mullite: ⟨022⟩, ⟨201⟩, ⟨111⟩, ⟨310⟩, ⟨130⟩) and of course the frequencies in 3:2 mullite are lower.

Hence it can be concluded that 2:1 and 3:2 mullite have very similar ordering schemes of oxygen vacancies and the real structures can be described via intervacancy correlation vectors (with slightly different frequencies).

5. Discussion

Videographic 3D simulations were performed for 2:1 and 3:2 mullite, whose Fourier transforms reproduced

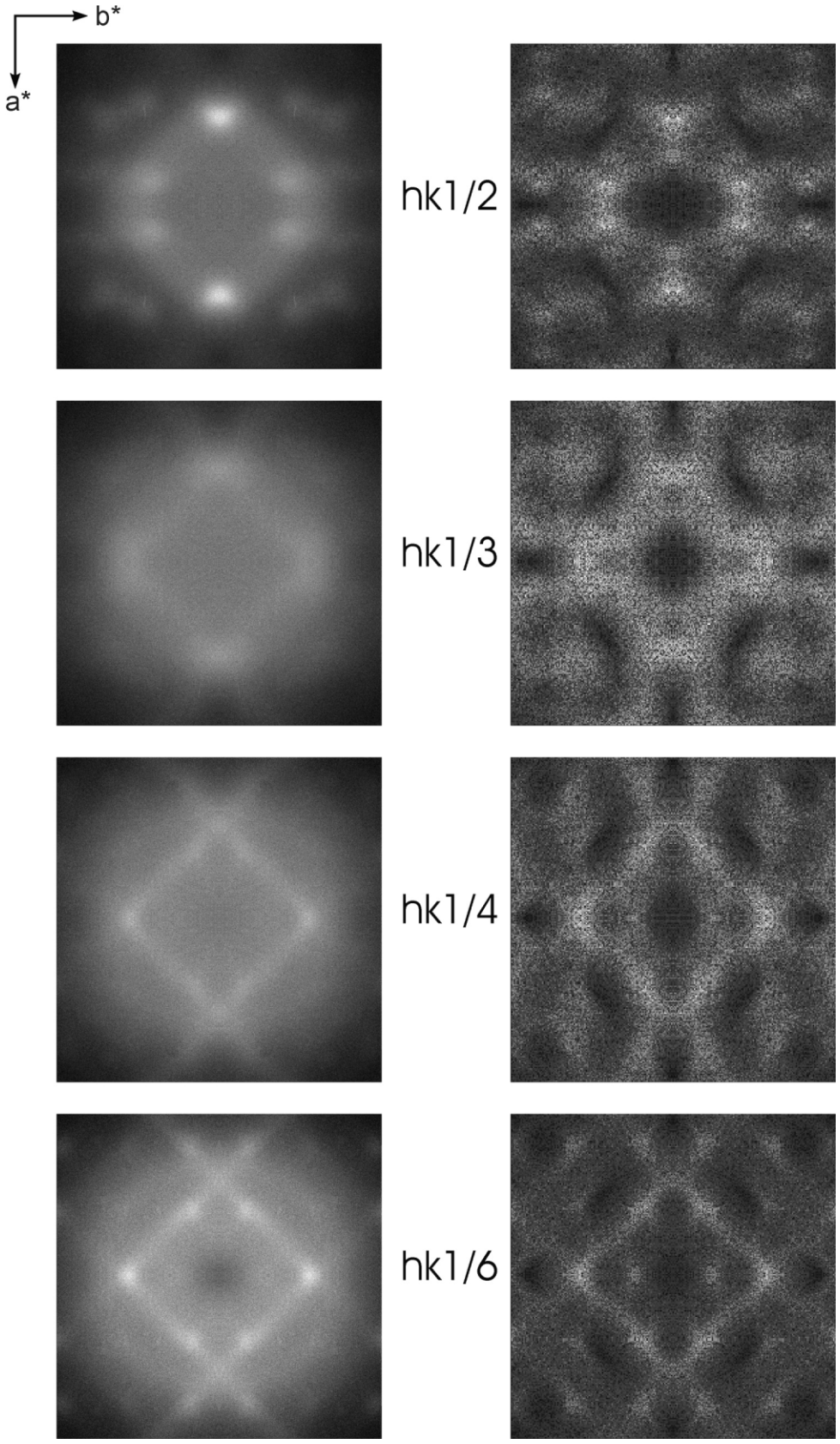

Fig. 6. (Left) X-ray diffraction patterns of 3:2 mullite; (right) Fourier transforms of the 3D simulation of 3:2 mullite.

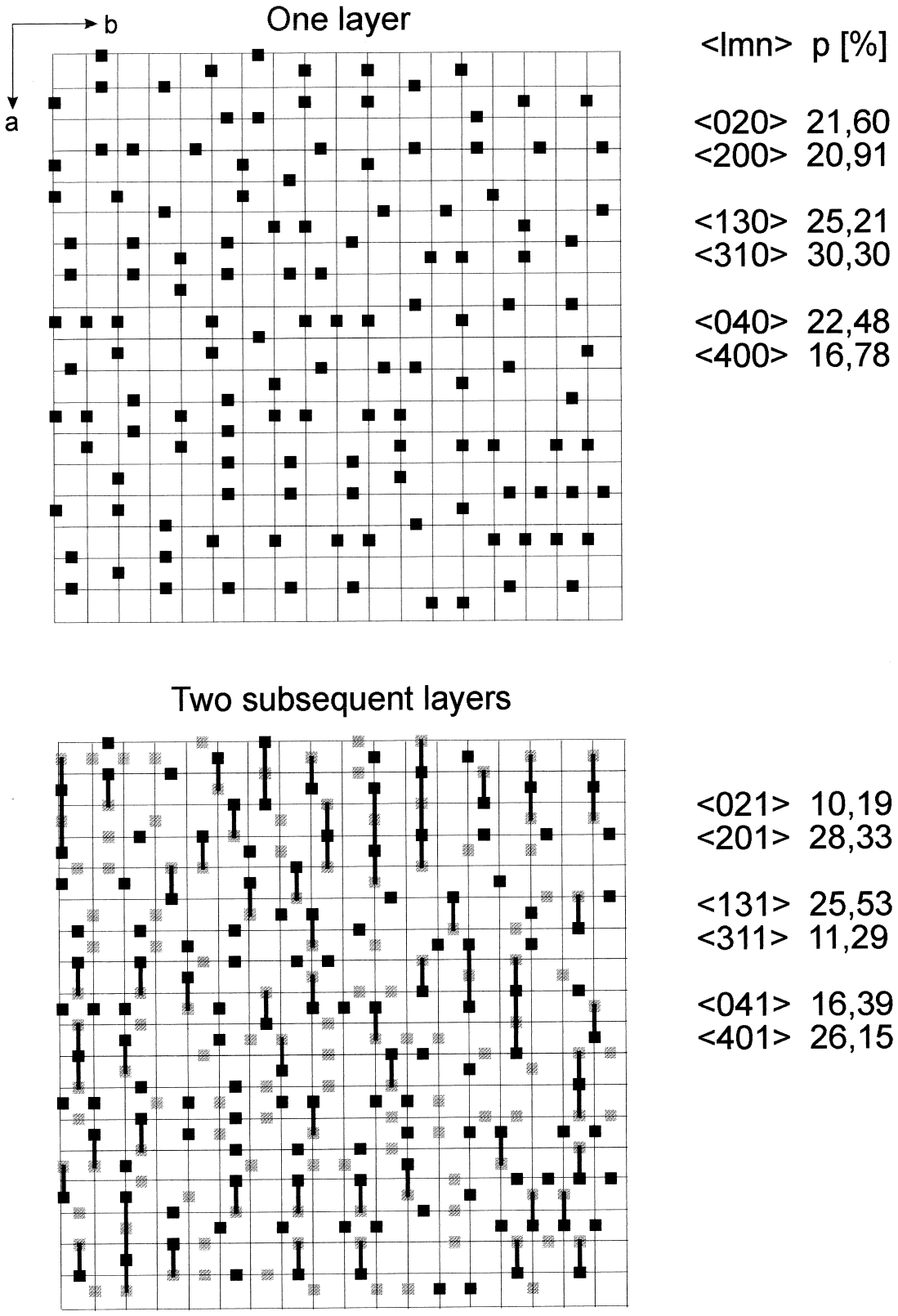

Fig. 7. Part of the simulation field for 2:1 mullite.

the diffuse scattering in all examined reciprocal planes as observed in the experimental patterns. By analyzing the 3D simulation fields the vacancy distribution in 2:1 and 3:2 mullite could be described completely in terms of correlation vectors. For this reason mullite is the first non-metallic mineral in which the diffuse scattering can be completely explained by short-range ordering. Unlike alloys the short-range ordering process in mullite is related to vacancies.

The knowledge of the real structure may help to explain some physical properties of mullite. In a part of the simulation field for 2:1 mullite (Fig. 7) differences in the vacancy arrangements along the *a*- and the *b*-axis can be observed. In one *ab*-layer (Fig. 7 top) the differences in probabilities of correlation vectors (p_{lmn}) are small: There are linear arrangements along the *a*-axis with the vectors ⟨200⟩ and ⟨130⟩ as well as linear arrangements along the b-axis with the vectors ⟨020⟩ and ⟨310⟩. The frequencies of ⟨200⟩ and ⟨020⟩ are very similar, the vector ⟨310⟩ is more frequent than ⟨130⟩, but both are preferred. However, for a proper description of the physical behaviour of a bulk crystal it is more realistic to consider not only one layer with correlation vectors lm0 but at least two subsequent layers. The superposition of two subsequent layers (Fig. 7 bottom) with the correlation vectors *lm* 0 and *lm* 1 clearly shows differences in the vacancy arrangements (concentrations) in projection on the *a*- and *b*-direction: The vector ⟨201⟩ is very frequent (marked with black lines in Fig. 7), however, the vector ⟨021⟩ is rare, and ⟨131⟩ is frequent, ⟨311⟩ rare. Therefore the dependence of several physical properties on the direction (for example the thermal expansion coefficient[12]) may be explained with the given distribution of oxygen vacancies, which can be well described with the help of intervacancy correlation vectors.

References

1. Rahman, S. H., Strothenk, S., Paulmann, C. and Feustel, U., Interpretation of mullite real structure via inter-vacancy correlation vectors. *J. Eur. Ceram. Soc*., 1996, **16**, 177–186.
2. McConnell, J. D. C. and Heine, V., Incommensurate structure and stability of mullite. *Phys. Rev*., 1985, **B31**, 6140–6142.
3. Angel, R. J. and Prewitt, C. T., The incommensurate structure of mullite by patterson synthesis. *Acta Crystallogr*., 1987, **B43**, 116–126.
4. Angel, R. J., McMullan, R. K. and Prewitt, C. T., Substructure and superstructure of mullite by neutron diffraction. *Am. Mineral*., 1991, **76**, 332–342.
5. Rahman, S. H., *Die videographische Methode: Ein neues Verfahren zur Simulation und Rekonstruktion fehlgeordneter Kristallstrukturen*. Universität Hannover, Habilitationsschrift, 1991.
6. Rahman, S. H., Paulmann, C. and Strothenk, S., 3-D Characterization of the Oxygen Vacancy Distribution in Mullite with HREM and the Videographic Method. Abstracts, 1994 ECM-15 Dresden.
7. Butler, B. D. and Welberry, T. R., Analysis of diffuse scattering from the mineral mullite. *J. Appl. Cryst*., 1994, **27**, 742–754.
8. Welberry, T. R. and Butler, B. D., Local structural information of mullite obtained from diffuse X-ray scattering. *J. Eur. Ceram. Soc*., 1996, **16**, 187–193.
9. Rahman, S. H., The videographic method: a new procedure for the simulation and reconstruction of real structures. *Acta Crystallogr*., 1993, **A49**, 56–68.
10. Rahman, S. H. and Rodewald, M., Simulation of short range order in FCC-alloys. *Acta Crystallogr*., 1995, **A51**, 153–158.
11. Brunauer, G., Frey, F., Boysen, H. and Schneider, H., High-temperature thermal expansion of mullite: an in situ neutron diffraction study up to 1600°. *J. Eur. Ceram. Soc*., 2001, **21**(14), 2563–2567.
12. Schneider, H., Thermal expansion of mullite up to 1600 °C. *J. Eur. Ceram. Soc*., 2001, in press.
13. Angel, R. J. and Prewitt, C. T., Crystal structure of mullite: a re-examination of the average structure. *Am. Mineral*., 1986, **71**, 1476–1482.